AIAA JOURNAL
Vol. 41, No. 1, January 2003

Mechanism of Shock Wave Oscillation in Transonic Diffusers

Taro Handa* and Mitsuharu Masuda†
Kyushu University, Fukuoka 816-8580 Japan
and
Kazuyasu Matsuo‡
University of Kitakyushu, Fukuoka 808-0135 Japan

Self-excited shock wave oscillation in a two-dimensional transonic diffuser is investigated experimentally and analytically. In the experiments, the temporal position of a shock wave is recorded by a high-speed charge-coupled device camera combined with a schlieren system, simultaneously measuring the fluctuation of the static pressure on the diffuser wall. The temporal variation of the static pressure is also measured to obtain the propagation of pressure disturbances. The results show that a pressure disturbance is generated near the stem of the shock wave and is convected in the downstream direction. In the downstream region where the boundary layer becomes highly turbulent, another disturbance is generated that propagates upstream and causes the shock wave to oscillate. One-dimensional Euler equations are solved numerically, and the power spectral density distribution of the shock wave oscillation is calculated. The numerical results agree very well with the experiments. It is also shown that the present calculation can explain the shock wave oscillation in the diffusers reported so far.

Nomenclature

A	=	cross-sectional area
a	=	sound velocity
e	=	total energy per unit volume
f	=	frequency
h	=	diffuser throat height
l	=	diffuser length measured from the throat
M	=	Mach number
p	=	pressure
R_{p-p}	=	correlation coefficient between measured static pressures
R_{p-x}	=	correlation coefficient between static pressure and shock wave position
t	=	time
t_d	=	delay time
u	=	velocity
x	=	streamwise coordinate
y	=	transverse coordinate
Δt	=	time step
γ	=	specific heat ratio
ρ	=	density

Subscripts

s	=	shock wave
1	=	value upstream of shock wave
2	=	value downstream of shock wave

Superscripts

$'$	=	fluctuating component
$\hat{}$	=	normalized by values at throat
$*$	=	throat value

Received 12 September 2001; revision received 19 June 2002; accepted for publication 20 August 2002.

*Research Associate, Department of Energy and Environmental Engineering, 6-1 Kasuga-Koen, Kasuga City; handa@ence.kyushu-u.ac.jp.

†Professor, Department of Energy and Environmental Engineering, 6-1 Kasuga-Koen, Kasuga City; masuda@ence.kyushu-u.ac.jp.

‡Professor, Department of Mechanical Systems and Environmental Engineering, 1-1 Hibikino, Wakamatsu-ku, Kitakyushu City; matsuo@env.kitakyu-u.ac.jp.

Introduction

A NORMAL shock wave in a diffuser interacts with the wall boundary layer and, even if the flow upstream of the shock wave is quiescent, oscillation of the shock wave is induced. Because this flow oscillation is of great practical importance, there is much reported work.[1–5]

A detailed experimental investigation of this problem was made by Sajben and Kroutil.[1] They tested the model B diffuser reproduced in Fig. 1a. Along with optical flow visualization by the schlieren method, they used a line-image sensor to measure the temporal variation of the shock wave location, and the displacement of the shock wave from its position averaged in time was analyzed. They controlled the boundary-layer thickness on the curved upper wall and found that the power spectral density distributions of the shock wave displacement depended strongly on the boundary-layer thickness. When the Mach number upstream of the shock wave was about 1.2 and boundary-layer separation did not occur, the peak of the power spectral density shifted to higher frequency as the boundary-layer thickness was increased; they called this "weak shock" flow. For flow with a Mach number of 1.31, on the other hand, the boundary layer was separated near the foot of the shock wave, and the boundary-layer thickness was found to have little effect on the power spectral density of the shock position fluctuations; this flow was called "strong shock" flow. In both cases, the power spectral density did not show a sharp peak and its distribution was relatively broad. This means that the flow was not "pulsating," namely, no distinctive frequency existed in the shock wave oscillation.

The Ref. 1 experiments were checked numerically by Liou and Coakley[2] by solving the time-dependent Navier–Stokes equations with the k–ω^2 two-equation turbulence model. Although they succeeded in reproducing the flow with an oscillating shock wave, the oscillation seemed regular, and the shock wave was seen to pulsate with a single distinctive frequency. In this respect, the calculation did not reflect the experimental results.

Bogar et al.[3] conducted another experimental investigation with the model G diffuser shown in Fig. 1b. In the weak shock flow with Mach number from 1.16 to 1.27, the power spectral density of the shock wave oscillation had several peaks, and the oscillation was seen to be confined to a narrow frequency range compared to the flow in model B. They also checked the effect of the length of the diffuser by changing the length of the constant area duct downstream of the diffuser and found that the oscillation depended on length; this was suspected to be caused by the acoustic resonance effect. When the Mach number was increased to the 1.27–1.35 range, the boundary layer was separated (strong shock flow) and the power spectral density of the shock-position fluctuations had a single peak.

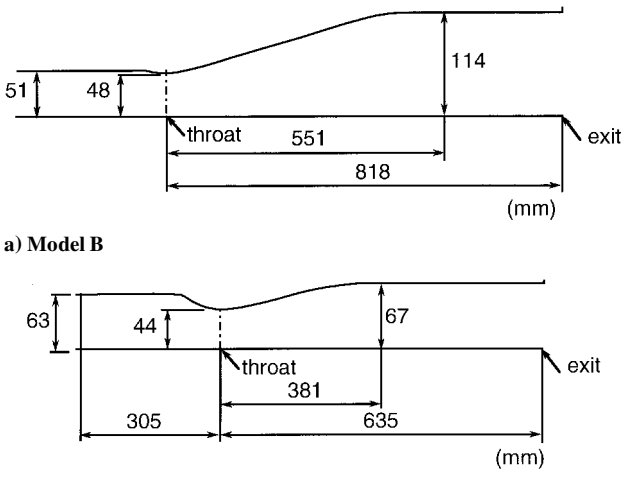

a) Model B

b) Model G

Fig. 1 Diffusers used in Refs. 1 and 3.

Although they suspected that the oscillation frequency depended on the length of the core region downstream of the shock wave where viscous effects were neglected, very little was known about the mechanism of the shock wave oscillation.

The flow in the model G diffuser was calculated by Hsieh and Coakley.[4] Results suggested that the peak frequency depended on the diffuser length, but the peak frequency of the long diffuser did not agree with experiments.

Recently, Robinet and Casalis[5] applied quasi-one-dimensional linear stability analysis to the time-averaged flow calculated by the Navier–Stokes equations. The calculated oscillation frequency of the shock wave agreed very well with the flow in model G with a Mach number of 1.35. Because the theory took into account the reflection of disturbance waves at the diffuser exit, the frequency depended strongly on the diffuser length. Because of this consideration of the wave reflection, however, their method ceases to be valid for a flow that does not have a core region at the diffuser exit.

Despite the preceding efforts to understand shock wave oscillation in transonic diffusers, important problems remain unsolved. These are, first, what causes the shock wave oscillation; second, what determines the major oscillation frequency; and finally, why does the power spectral density distribution of models B and G differ?

Experimental and analytical work was conducted aimed at answering these questions. In the experiments, the shock wave position in a diffuser was measured by a high-speed charge-coupled device (CCD) camera combined with the schlieren method, and the static pressure fluctuations along the flat wall were measured simultaneously. The temporal variation of the static pressure on the side wall was also measured to obtain the propagation of pressure disturbances. Along with the results of these experiments, the time-dependent quasi-one-dimensional Euler equations were solved numerically by the total variation diminishing (TVD) method, and the resulting power spectral density distributions of the shock wave displacements were compared with those measured experimentally.

Experimental Setup and Results

Experimental Setup

Figure 2 shows the supersonic indraft wind tunnel used in the present experiments. This consists of the 18-m^3 reservoir tank, test channel, 0.5-m^3 settling chamber, and 15-m^3 vacuum tank. The working gas is atmospheric air, the relative humidity of which is reduced to prevent condensation in the test channel. The vacuum tank is evacuated before the experiments to a pressure of less than 13 kPa by closing the valve shown in Fig. 2. The flow is started by opening the valve and introducing the dry air contained in the reservoir tank into the test channel. The air is then discharged into the settling chamber. The shock wave location is adjusted by a wedge inserted in the duct downstream of the test channel.

The flowfield is visualized by the schlieren method. A spark light source with a duration time of 20 ns is used to take instantaneous schlieren photographs. A continuous light source (150-W tungsten lamp) is also used to obtain schlieren images by a high-speed CCD camera (Kodak, HS4540) with an acquisition rate of 18,000 frames/s. These schlieren images were digitized and stored into a personal computer. The computer then calculated the darkness of each image along the line $y = 8$ mm, and the displacement of the shock wave from its time-averaged position was determined.

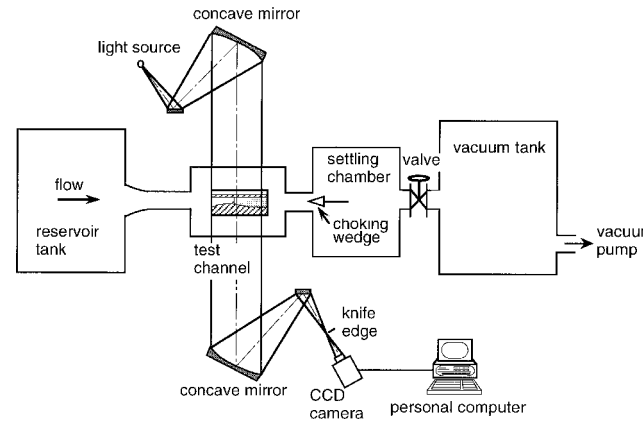

Fig. 2 Experimental setup.

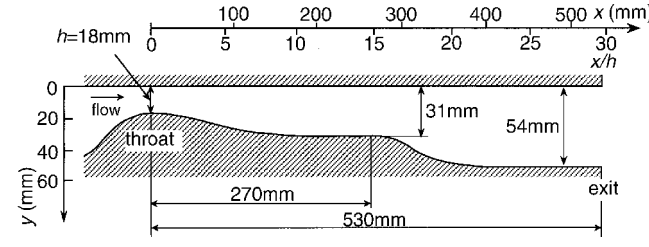

Fig. 3 Test diffuser.

The upper wall has several static pressure holes with pressure transducers (Kulite XCQ-062), and the temporal variation of the static pressure is measured simultaneously with the high-speed schlieren images. The temporal variation of the pressure on the side wall is also measured by the pressure transducers (Kulite XCS-190) to obtain the propagation of pressure disturbances.

The diffuser used in the present experiments is shown in Fig. 3. This is two dimensional in shape with 40-mm depth having a straight upper wall. The throat height is 18 mm. In the divergent part, the contour of the lower wall is determined by the method of characteristics, so that, if the flow is inviscid, it is uniform and no expansion or compression wave exists at the exit. The diffuser is smoothly connected to a duct 54 mm in height. The location of a shock wave is adjusted by inserting a wedge at the exit of this duct. The x and y in Fig. 3 are the streamwise and transverse coordinates, respectively; the origin is taken at the throat position on the upper wall.

Time-Averaged Flow in the Diffuser

Streamwise distributions of the time-averaged static pressure on the upper wall were measured in the preliminary experiments. In addition to this, a time-averaged position of the shock wave was obtained by the high-speed schlieren images. These results enabled calculation of the Mach number M_1 in front of the shock wave at the time-averaged position by assuming that the flow is one dimensional and isentropic in the region upstream of the shock wave. In the present experiments, M_1 was varied from 1.26 to 1.48. The Reynolds number based on the throat condition was 2.6×10^5.

Typical schlieren photographs are shown in Figs. 4a and 4b. As expected, the flow pattern depends strongly on the Mach number M_1. For the flow with $M_1 = 1.26$ (Fig. 4a), the shock wave is seen to be generated just downstream of the geometrical throat, and the thickness of the boundary layer both on the top and bottom walls increases abruptly immediately behind the shock wave. It does not seem possible to determine definitively whether the boundary layer is separated or not downstream of the shock wave, but the separation, if it exists, is not strong, and the flow corresponds to the weak shock

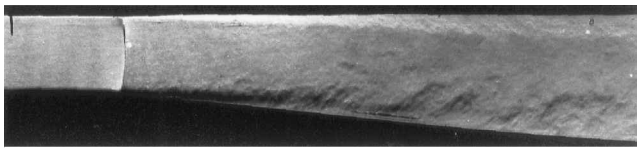

a) $M_1 = 1.26$

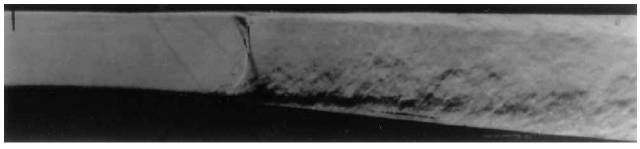

b) $M_1 = 1.48$

Fig. 4 Schlieren photographs.

case. When the Mach number is increased to 1.48 (Fig. 4b), the shock wave becomes stronger and separates the boundary layer that develops along the bottom wall. The shock wave is also seen to be bifurcated near the bottom wall, and this is the strong shock flow.

Propagation of a Pressure Disturbance

To examine the propagation of a pressure disturbance, the temporal variation of the pressure on the side wall was measured. The results for the flow with $M_1 = 1.48$ are shown in Fig. 5. Figure 5 consists of six parts; the horizontal distance is common to all and is shown in Fig. 5f as x/h, where x is the distance measured from the geometrical throat and h the throat height, respectively. Figure 5a shows the probability density function of the shock wave displacement, indicating that the time-averaged position of the shock wave is $x/h \sim 3.0$. A typical schlieren photograph is shown in Fig. 5e, where the pressure hole positions are indicated by white dots. The pressure was measured along the lines A, B, and C, and the cross-correlation coefficient R_{p-p} on each line was calculated between the measured pressure at each pressure hole and the pressure at the location denoted by the reference point in the photograph. The calculated R_{p-p} distributions are plotted by taking the delay time t_d as an ordinate.

Line A is taken along the flat upper wall, and the results are shown in Fig. 5b. Upstream of the time-averaged shock wave position $x/h \sim 3.0$, the curves of R_{p-p} are almost flat, but the R_{p-p} curve has a positive peak at $x/h = 3.0$, and the position t_d of this positive peak decreases with x/h until about $x/h = 5.0$; it then increases again in the downstream region. The R_{p-p} distributions along line B in Fig. 5c is also flat for $x/h < 3.0$, but it has two peaks in the region $3.0 < \sim x/h < \sim 5$. The position t_d of the peak in the positive t_d region decreases and that in the negative t_d region increases with x/h. For $x/h > \sim 5.0$, R_{p-p} has only one peak, and the t_d of this peak increases with x/h. The R_{p-p} distributions along line C are shown in Fig. 5d. For $x/h < 3.0$, R_{p-p} also has no peak. A single peak appears at $x/h \sim 3.0$, and in the case the position t_d of this peak increases almost linearly with x/h. These results indicate that a pressure disturbance is generated near the stem of the shock wave on the lower wall ($x/h \sim 3$) due to boundary-layer separation and is convected downstream. The convection speed calculated from the peak in the cross-correlation distributions is about 140 m/s. In addition to this, another disturbance is generated at $x/h \sim 5.0$ and is propagated upstream with a speed of about 40 m/s in the upper part of the diffuser; this speed is in accordance with the difference between the speed of sound and the flow velocity downstream of the normal shock wave ($u - a$). Figure 5 corresponds to a strong shock flow with large boundary-layer separation at the lower stem of the shock wave. We also tested the flow with $M_1 = 1.26$, where the boundary-layer separation was not as strong as for the $M_1 = 1.48$ flow. The cross-correlation coefficients of these two flows were found to be almost identical.

For the weak shock flow in the model G diffuser shown in Fig. 1b (Ref. 3), the existence of a standing wave was suggested by the cross-correlation coefficient between the shock wave position and the static pressure along the curved wall, namely, the peak of the correlation coefficient distribution changed sign at the node.[3] The

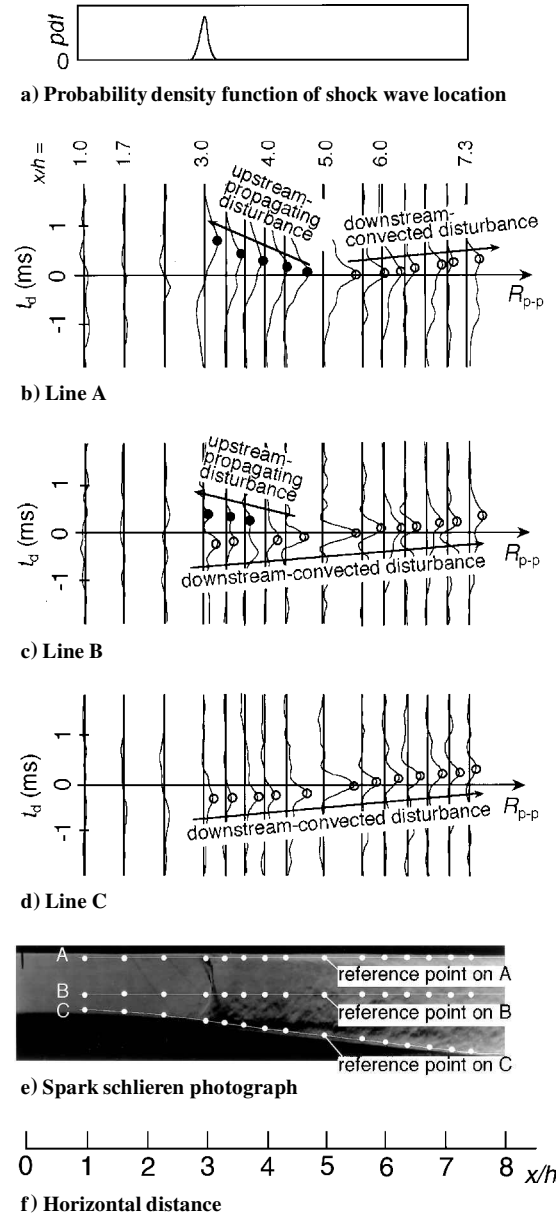

Fig. 5 Cross-correlation coefficients of static pressures on the side wall ($M_1 = 1.48$).

present results, however, do not have an indication of a standing wave, so that acoustic resonance may not play an important role for shock wave oscillation in the present flow. For the strong shock flow in the model G, the cross-correlation coefficient took a trend similar to that shown in Fig. 5d, suggesting that a disturbance was convected downstream in the boundary layer.[3] This, however, was taken along the curved wall, where boundary-layer separation at the stem of the shock wave was strong compared to that along the flat wall; no data are available in Ref. 3 on the behavior of the cross-correlation coefficient along the flat wall.

Figure 5b seems to indicate that the shock wave oscillation is caused by a pressure disturbance that is generated near $x/h = 5.0$ and is propagated upstream on the flat upper wall. The cross-correlation coefficient R_{p-x} is, therefore, calculated between the measured temporal variation of the static pressures on the upper wall and the displacement of the shock wave from its time-averaged position obtained from the high-speed schlieren images.

The result for the flow with $M_1 = 1.48$ is shown in Fig. 6. The R_{p-x} distributions are seen to take a negative peak near the time-averaged position of the shock wave $x/h = 3.0$. Downstream of $x/h = 3.0$, this negative peak moves to the positive t_d direction with the increase in x/h, and in the region $x/h \geqq 5.4$, the position of the negative peak becomes constant. This behavior of R_{p-x} suggests that

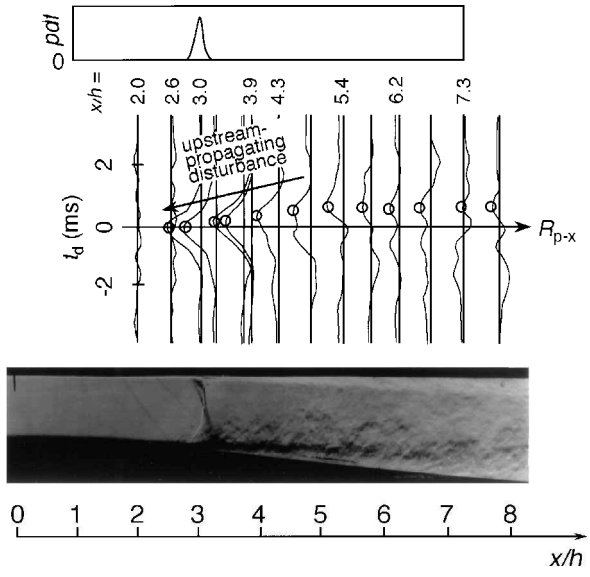

Fig. 6 Cross-correlation coefficients of the top wall static pressure with shock displacement ($M_1 = 1.48$).

the shock wave is forced to oscillate by a pressure disturbance generated in the vicinity of $x/h = 5.4$. The change in t_d at the peak R_{p-x} with x/h also gives the propagation velocity of a disturbance. The estimated velocity is about 50 m/s; this value is consistent with that calculated from the difference between the flow velocity and the sound velocity behind the shock wave. In the region upstream of the shock wave, $x/h = 2.6$ and 2.0, the cross-correlation coefficient does not have a peak; this implies that a disturbance in the region upstream of the shock wave is not responsible for the oscillation. Although not shown, measurements were made for the flow with $M_1 = 1.26$, and similar results were obtained.

As already mentioned, the schlieren images were taken with a high-speed CCD camera and also with a conventional camera and spark light source. Closer inspection of these images indicates that the dark part moves violently at $x/h \sim 5$. This means that a highly unsteady flow with large density gradients exists in this region. In the downstream region $x/h \sim 7$, however, the darkness of the schlieren image, hence, the density gradient, decreases probably because of the breakdown of vortices. This observation suggests that the boundary layer on the curved bottom wall becomes highly turbulent near the position $x/h \sim 5$; this unsteady boundary layer is probably responsible for the generation of the pressure disturbance.

Numerical Simulation

Method of Analysis

As described earlier, a shock wave oscillation seems to be caused by a pressure disturbance generated in the region where the boundary layer on the curved wall is highly turbulent. Therefore, the numerical analysis is attempted to see the response of a shock wave interacting with a pressure disturbance.

The basic equations are the quasi-one-dimensional Euler equations. When it is assumed that the gas is perfect, the conservation equations of mass, momentum, and energy are written as

$$\frac{\partial \rho}{\partial t} + \frac{\partial (\rho u)}{\partial x} + \frac{\rho u}{A}\frac{\mathrm{d}A}{\mathrm{d}x} = 0 \tag{1}$$

$$\frac{\partial (\rho u)}{\partial t} + \frac{\partial (\rho u^2 + p)}{\partial x} + \frac{\rho u^2}{A}\frac{\mathrm{d}A}{\mathrm{d}x} = 0 \tag{2}$$

$$\frac{\partial e}{\partial t} + \frac{\partial [(e + p)u]}{\partial x} + \frac{(e + p)u}{A}\frac{\mathrm{d}A}{\mathrm{d}x} = 0 \tag{3}$$

respectively, where the total energy per unit volume e is

$$e = p/(\gamma - 1) + \tfrac{1}{2}\rho u^2 \tag{4}$$

The diffuser is assumed two dimensional, and the cross-sectional area depends only on diffuser height. The gas is air with $\gamma = 1.402$. Equations (1–3) are solved by the second-order symmetric TVD scheme.[6] Calculations are started from a steady-state solution estimated by the one-dimensional adiabatic theory for the assigned time-averaged pressure at the exit $\bar{p}_{\mathrm{exit}}$. The calculation proceeds with a normalized time-step $\Delta t/(h/a) = 9.0 \times 10^{-4}$ with Courant number equal to 0.87.

To obtain the shock wave oscillation, a numerical pressure disturbance should be imposed as white noise in the flow. When the preceding experimental results are considered, the location where a pressure disturbance is generated is deduced from the cross correlation of the static pressures as $x/h = 4.0$ for $M_1 = 1.26$ and $x/h = 5.0$ for $M_1 = 1.48$. In the model B and G diffusers,[1,3] this location is assumed to be where the static pressure fluctuations are maximum. The amplitude of the disturbance is determined from the condition that the calculated amplitude of the shock wave oscillation fits the experiments.

At the downstream boundary, the pressure, density, and velocity are assumed to have no gradient in the flow direction. According to this condition, no disturbance wave is reflected at the downstream boundary. For the present diffuser and model B, the downstream boundary is set at the location denoted exit in Figs. 3 and 1a, respectively. In the model G diffuser, on the other hand, it seemed necessary to take the reflection effect into account. The cross-sectional area is, therefore, assumed to increase rapidly with x downstream of the exit ($x = x_{\mathrm{exit}}$) shown in Fig. 1b as

$$A(x) = A_{\mathrm{exit}} \exp[C(x - x_{\mathrm{exit}})/h], \qquad (x - x_{\mathrm{exit}})/h \le 2$$

$$A(x) = A_{\mathrm{exit}} \exp[2C], \qquad (x - x_{\mathrm{exit}})/h > 2 \tag{5}$$

where C is a constant set as 0.6; this ensures a rapid but continuous increase in cross-sectional area. Although this shape is taken arbitrarily to simulate a sudden increase in cross-sectional area, it is necessary for the numerical solutions to converge. Then when the no-gradient boundary condition far downstream of x_{exit} is applied, a disturbance wave is made, which is reflected at x_{exit}.

Comparison of Calculations with Experiments

The power spectral density of the shock wave displacement from its time-averaged position was calculated by the described method and compared with that obtained experimentally by analyzing the high-speed schlieren images. Results for the diffuser used in the present experiments are plotted in Fig. 7, where the experimental and calculated results are shown by dotted and solid lines, respectively. In Fig. 7, $f \cdot S(f)$ is plotted as a function of $\ell n\, f$. Therefore, the area under a given curve segment $f \cdot S(f)\delta(\ell n\, f)$ corresponds to the intensity of the respective frequency range.[1] Over the measured frequency range, the area under the calculated curve is adjusted to be equal to that for the experiments. Note that, due to the boundary layer, we did not match the Mach numbers used in the calculations to those in the experiments; instead the Mach numbers were selected so that the calculated shock wave position averaged in time agreed with experiments. The Mach numbers in the calculations were 1.31 and 1.55 for Figs. 7a and 7b, respectively. We have checked that this difference in Mach numbers did not cause any appreciable difference in the power spectral density distributions. As shown in Fig. 7, the profiles of calculated power spectral density distributions agree remarkably well with experimental results; the agreement of the peak oscillation frequency is particularly good. Thus, the calculations support the experimental observation that the shock wave oscillation in the present experiments is caused by an upstream-propagating pressure disturbance generated in the region where the boundary layer on the curved wall is highly turbulent. Although results are not shown, we calculated these flows by taking into account a wave reflection at the downstream boundary, but the resulting power spectral density differed greatly from experiments. This again suggests that, in the present diffuser, a pressure disturbance reflected at the exit, compared to that produced in the diffuser by the turbulent boundary layer, is small enough that it does not affect the shock wave oscillation.

Sajben and Kroutil[1] studied experimentally the flow in the model B diffuser (Fig. 1a) by changing the displacement thickness of the boundary layer on the curved wall. The dotted lines in Fig. 8 are

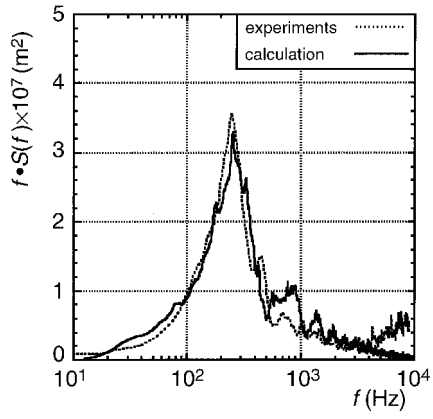

a) $M_1 = 1.26$

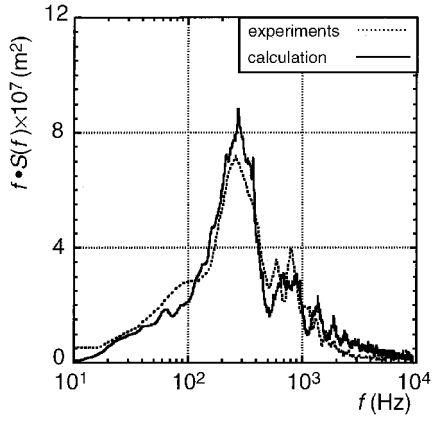

b) $M_1 = 1.48$

Fig. 7 Power spectral density of shock wave displacement for the present diffuser.

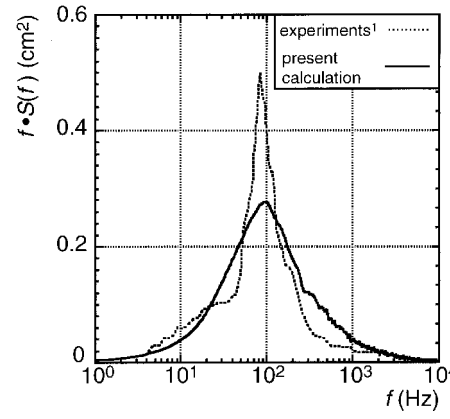

a) $M_1 = 1.20$

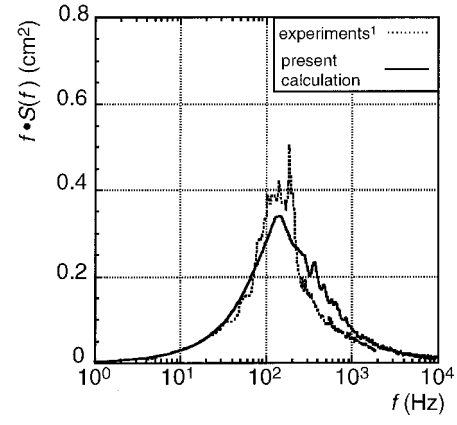

b) $M_1 = 1.31$

Fig. 8 Power spectral density of the shock wave displacement for model B diffuser[1] with 2.0% inlet blockage on the top wall.

their results. We calculated the power spectral densities of the shock wave displacement for these flows with the no-reflection boundary condition. In Fig. 8, their experiments for the inlet blockage at the throat of 2.0% are compared with our calculated results. As shown here, our calculations are found to fit their experiments very well.

Bogar et al.[3] conducted other experiments for the flow in the model G diffuser (Fig. 1b). The typical result is shown as a dotted line in Fig. 9. This differs very much from Figs. 7 and 8 in that the width of the power spectral density profile is much narrower than for the present experiments, as well as for the model B flows. We calculated this flow first with the no-reflection boundary condition, but, similar to Fig. 7 or 8, the width of the power spectral density was broad and did not match the experiments. Calculations were then conducted with the reflection boundary condition described earlier. As shown by the solid line, the results exhibit a narrow peak at 200 Hz, which agrees with the experiments. (In Fig. 9, the calculated results are plotted by adjusting the peak height at 200 Hz to the experiments.) These calculations, on the other hand, did not include the blockage effect of the boundary layer, so that we next tried to incorporate this effect into our numerical analysis by using the effective cross-sectional area instead of the geometrical area of the diffuser. Robinet and Casalis,[5] in their analysis of the model G flow, obtained the time-averaged streamwise velocity distribution by solving the Navier–Stokes equations numerically. By the use of their results, the effective cross-sectional area was estimated, and the flowfield was calculated by the present method. The results are shown by a broken line in Fig. 9. Although the calculated results have several peaks that are not in the experiments, the shape of the major peak near 200 Hz agrees remarkably well with experiments. It is difficult to explain why peaks other than that at 200 Hz were not observed in the experiments. Closer examination of the high-speed video frames taken by the schlieren indicates that the flow downstream of the shock wave is highly turbulent, and large vortices are produced and convected in the downstream region. This unsteady behavior may give an answer to this question.

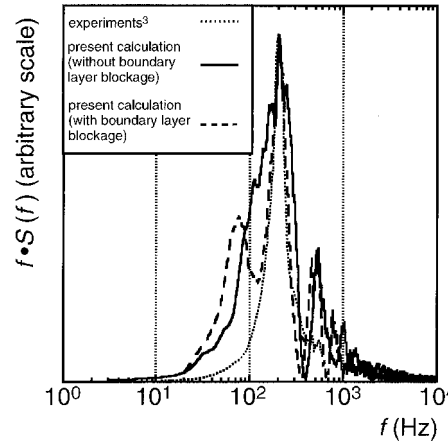

Fig. 9 Power spectral density of shock wave displacement for model G diffuser[3] (data reproduced from Ref. 3).

We shall next consider the behavior of the dominant oscillation frequency of the shock wave in the present and model B and G diffusers.

In the model-G-type flow, the reflection of a pressure disturbance at the exit is very important in determining the dominant oscillation frequency. This, in turn, means that the oscillation frequency depends on the diffuser length. Taking the model G flow as an example, we calculated this effect for $M_1 = 1.35$. The results are shown in Fig. 10, which also includes the experiments,[7] two-dimensional numerical simulation,[4] and linear stability theory.[5] The present calculations, denoted by open circles, open triangles and open rectangles, are obtained by neglecting the boundary-layer blockage effect, and agree with the simple acoustic analysis by Bogar et al.[3] when $l/h > 20$. Disagreement among these results occurs for shorter

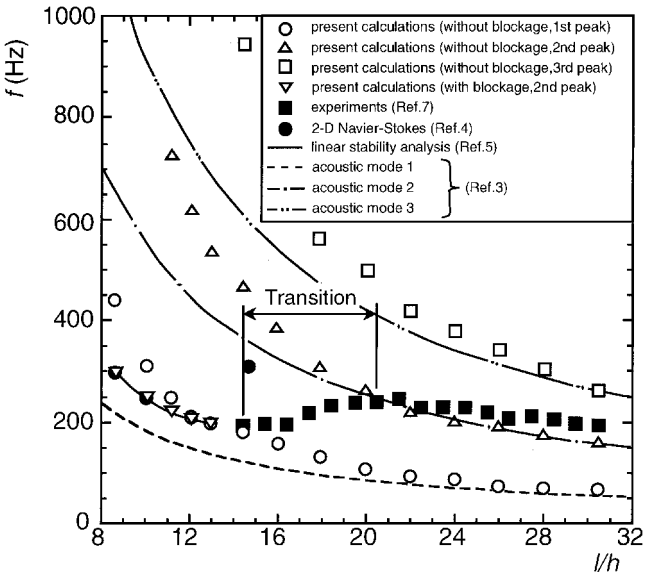

Fig. 10 Frequency vs diffuser length (model G).

diffusers; this is probably caused by the effect that a pressure disturbance is partly reflected by the diverging part of the diffuser wall. Note also that the present calculations with the boundary-layer blockage effect coincide very well with the linear stability analysis and Navier–Stokes solutions for $l/h < 13$. As shown in Fig. 10, the present calculations seem to explain the experimental results by Bogar et al. very well. Although the reason why "transition" (Fig. 10) occurs is not clear, the results suggest that, for the model-G-type flow, the acoustic resonance effect determines the dominant oscillation frequency of the shock wave.

As already described, the present experiments had similar behavior to the model B flow, and the power spectral density was well explained by the numerical analysis with the no-reflection boundary condition. In the following, we shall extend an analytical method developed by Culick and Rogers[8] to calculate the dominant frequency of the shock wave oscillation in this case. This procedure clarifies the physical mechanism of the shock wave oscillation in the present diffuser flow.

Assume that a pressure disturbance propagating upstream moves a normal shock wave from position x_s to $x_s + x_s'$. When the second order quantities are neglected, the pressures and Mach number can be expressed as

$$p_1(x_s + x_s') = p_1(x_s) + \frac{\mathrm{d}p_1}{\mathrm{d}x}x_s' \tag{6}$$

$$p_2(x_s + x_s') + p_e' = p_2(x_s) + \frac{\mathrm{d}p_2}{\mathrm{d}x}x_s' + p_e'(t) \tag{7}$$

$$M_1(x_s + x_s') = M_1(x_s) + \frac{\mathrm{d}M_1}{\mathrm{d}x}x_s' \tag{8}$$

where p_1 and p_2 are the pressures upstream and downstream of the shock wave, p_e' is the disturbance pressure, M_1 is the Mach number in front of the shock wave, and t is time. The parameters are then normalized as

$$\hat{x} = x/h, \qquad \hat{t} = t/(h/a^*), \qquad \hat{f} = f/(a^*/h)$$
$$\hat{A} = A/A^*, \qquad \hat{p} = p/p^*, \qquad \hat{a} = a/a^* \tag{9}$$

Although the shock wave is not stationary but moves with the speed of $\mathrm{d}\hat{x}_s/\mathrm{d}\hat{t}$, it is also assumed that the Rankine–Hugoniot relation is satisfied across the shock wave. When the preceding equations are substituted into the Rankine–Hugoniot relation for the moving shock wave and the second-order perturbation terms are neglected,

$$\frac{\mathrm{d}\hat{x}_s'}{\mathrm{d}\hat{t}} + \frac{1}{\hat{\tau}}\hat{x}_s' = \frac{C}{\hat{\tau}}\hat{p}_e' \tag{10}$$

where

$$\hat{\tau} = -\frac{1}{\hat{a}_1 P_s}\left(\frac{1}{\hat{A}}\frac{\mathrm{d}\hat{A}}{\mathrm{d}\hat{x}}\right)^{-1}\left(\frac{\hat{p}_1}{\hat{p}_2}\right)\frac{4\gamma M_1}{\gamma+1} \tag{11}$$

$$C = \frac{1}{\hat{p}_2 P_s}\left(\frac{1}{\hat{A}}\frac{\mathrm{d}\hat{A}}{\mathrm{d}\hat{x}}\right)^{-1} \tag{12}$$

$$P_s = \frac{\mathrm{d}\ell n\,\hat{p}_1}{\mathrm{d}\ell n\,\hat{A}} - \frac{\mathrm{d}\ell n\,\hat{p}_2}{\mathrm{d}\ell n\,\hat{A}} + \frac{2\gamma}{\gamma+1}\frac{\hat{p}_1}{\hat{p}_2}\frac{\mathrm{d}\ell n M_1^2}{\mathrm{d}\ell n\,\hat{A}} \tag{13}$$

If the pressure behind a shock wave is assumed to be recovered isentropically, P_s is calculated as

$$P_s = -\frac{\gamma\left[M_1^2(\gamma-1)+2\right]}{(\gamma+1)\left(M_1^2-1\right)} - \frac{\gamma M_1^2\left[2M_1^2-(\gamma+3)\right]}{\left(M_1^2-1\right)\left[2\gamma M_1^2-(\gamma-1)\right]} \tag{14}$$

Equation (10) can be solved for the initial condition $\hat{x}_s' = 0$ at $\hat{t} = 0$ as

$$\hat{x}_s'(t) = \frac{C}{\hat{\tau}}e^{-\hat{t}/\hat{\tau}}\int_0^{\hat{t}} e^{\hat{t}'/\hat{\tau}}\hat{p}_e'(\hat{t})\,\mathrm{d}\hat{t}' \tag{15}$$

To understand the dependence of the dominant frequency on the various parameters involved in Eq. (15), the displacement $\hat{x}_s'$ is calculated by assuming a pressure disturbance with a single frequency as

$$\hat{p}_e'(t) = \varepsilon\hat{p}_2\cos 2\pi\hat{f}\hat{t} \tag{16}$$

where ε is a small value. This $\hat{p}_e'$ is substituted into Eq. (15), and the resulting equation is integrated to give

$$\hat{x}_s'(\hat{t}) = \frac{C\varepsilon\hat{p}_2}{1+(2\pi\hat{f}\hat{\tau})^2}\left[\sqrt{1+(2\pi\hat{f}\hat{\tau})^2}\cos(2\pi\hat{f}\hat{t}-\theta) - e^{-\hat{t}/\hat{\tau}}\right] \tag{17}$$

The mean-squared displacement is then calculated as

$$\hat{x}_{s,\mathrm{rms}}'^2 = \frac{(C\varepsilon\hat{p}_2)^2}{2[1+(2\pi\hat{f}\hat{\tau})^2]} \tag{18}$$

The frequency that maximizes the $\hat{f}\cdot\hat{x}_{s,\mathrm{rms}}'^2$ [equivalent to $\hat{f}\cdot S(\hat{f})$] is then obtained as

$$\hat{f}_p = 1/2\pi\hat{\tau} \tag{19}$$

Equation (19) gives the normalized peak frequency of the shock wave oscillation as a function of $\hat{\tau}$. Equation (19) is calculated, and the results are shown in Fig. 11 by a solid line. This includes

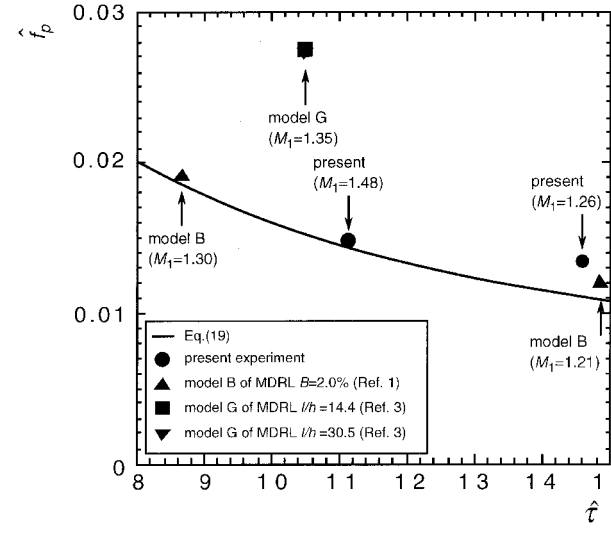

Fig. 11 Peak frequency vs the parameter $\hat{\tau}$.

the present experimental results as well as those for the model B and G flows. As shown in Fig. 11, the present experiments and the model B flow agree quite well with the theoretical prediction. When it is considered that in this theory the frequency is a function only of $\hat{\tau}$ and that the theory does not take the wave reflection at the diffuser exit into account, this agreement is an indication that the oscillation frequency of the shock wave in these diffusers is determined solely by the geometrical shape and the Mach number in front of the shock wave. The experimental results for model G, on the other hand, do not agree with the theoretical prediction. This again indicates that acoustic resonance, which is not taken into account in the theory, is an important mechanism for determining the shock wave oscillation in the flows of model G.

Conclusions

Shock wave oscillation in transonic diffusers is investigated experimentally and theoretically. The static pressure measurements show that a pressure disturbance is generated near the shock wave stem on the curved wall and is convected downstream, whereas in the downstream region where the boundary layer on the curved wall becomes highly turbulent, another disturbance is generated, which propagates upstream and oscillates the shock wave.

The power spectral density of the shock wave displacement from its time-averaged position is measured by high-speed schlieren images. This is also analyzed theoretically by solving the one-dimensional Euler equations numerically with the TVD method. Detailed comparisons of the experimental results with the calculations reveal that two entirely different mechanisms exist for the shock wave oscillation. One is that the shock wave is forced to oscillate by a pressure disturbance generated at the region where the boundary layer becomes turbulent. In this flow, a disturbance reflected at the diffuser exit plays no part in determining the power spectral density of the shock-position fluctuations nor the peak oscillation frequency; instead, the oscillation is governed by the geometrical shape of the diffuser and the Mach number in front of the shock wave. The power spectral density distribution, in this case, becomes broad. The other mechanism is that the reflection of a disturbance at the diffuser exit determines the shock wave oscillation. The shape of the power spectral density is narrow in this flow.

These results, we hope, can give answers to the three questions posed in the Introduction.

References

[1]Sajben, M., and Kroutil, J. C., "Effects of Approach Boundary-Layer Thickness on Oscillating, Transonic Diffuser Flows Including a Shock Wave," AIAA Paper 80-0347, 1980.

[2]Liou, M.-S., and Coakley, T. J., "Numerical Simulation of Unsteady Transonic Flow in Diffusers," *AIAA Journal*, Vol. 22, No. 8, 1984, pp. 1139–1145.

[3]Bogar, T. J., Sajben, M., and Kroutil, J. C., "Characteristic Frequencies of Transonic Diffuser Flow Oscillations," *AIAA Journal*, Vol. 21, No. 9, 1983, pp. 1232–1240.

[4]Hsieh, T., and Coakley, T. J., "Downstream Boundary Effects on the Frequency of Self-Excited Oscillations in Transonic Diffuser Flows," AIAA Paper 87-0161, 1987.

[5]Robinet, J.-C., and Casalis, G., "Shock Oscillations in Diffuser Modeled by a Selective Noise Amplification," *AIAA Journal*, Vol. 37, No. 4, 1999, pp. 453–459.

[6]Yee, H., "Upwind and Symmetric Shock-Capturing Schemes," NASA TM 89464, 1987.

[7]Bogar, T. J., Sajben, M., and Kroutil, J. C., "Characteristic Frequencies and Length Scales in Transonic Diffuser Flow Oscillations," AIAA Paper 81-1291, 1981.

[8]Culick, F. E. C., and Rogers, T., "The Response of Normal Shocks in Diffusers," *AIAA Journal*, Vol. 21, No. 10, 1983, pp. 1382–1390.

M. Sichel
Associate Editor